ACS OMEGA

Article

Cite This: ACS Omega 2019, 4, 19350−19357

http://pubs.acs.org/journal/acsodf

Controlled Release of Naringin in GelMA-Incorporated Rutile Nanorod Films to Regulate Osteogenic Differentiation of Mesenchymal Stem Cells

Yangjie Shao,[†] Dongqi You,[†] Yiting Lou,[†,‡] Jianhua Li,[§] Binbin Ying,[‡] Kui Cheng,[∥] Wenjian Weng,[∥] Huiming Wang,*[,†] Mengfei Yu,*[,†,‡,§,∥] and Lingqing Dong*[,†,∥]

[†]The Affiliated Stomatologic Hospital, School of Medicine, Zhejiang University, Hangzhou 310003, Zhejiang Province, China

[‡]Department of Stomatology, The Affiliated Ningbo First Hospital, Zhejiang University, Ningbo 315010, Zhejiang Province, China

[§]Hangzhou Dental Hospital, Hangzhou 310006, Zhejiang Province, China

[∥]School of Materials Science and Engineering, State Key Laboratory of Silicon Materials, Zhejiang University, Hangzhou 310027, Zhejiang Province, China

ABSTRACT: Naringin, a Chinese herbal medicine, has been demonstrated to concentration-dependently promote osteogenic differentiation of mesenchymal stem cells (MSCs). However, it remains a challenge to load naringin on coatings for osteogenesis and further control the release kinetics. Here, we demonstrated that the release behavior of naringin on rutile nanorod films could be controlled by either mixing naringin with gelatin methacryloyl (GelMA) before spinning onto the films or soaking the obtained GelMA-incorporated films with the naringin solution to achieve the distinct degradation-type release and diffusion-type release, respectively. We further revealed that the naringin-loaded coatings facilitated adhesion, proliferation and late differentiation, and mineralization of MSCs. Our findings provided a novel strategy to engineer the coatings with controlled release of naringin and emphasized the bioactivity of naringin for the osteogenic differentiation of MSCs.

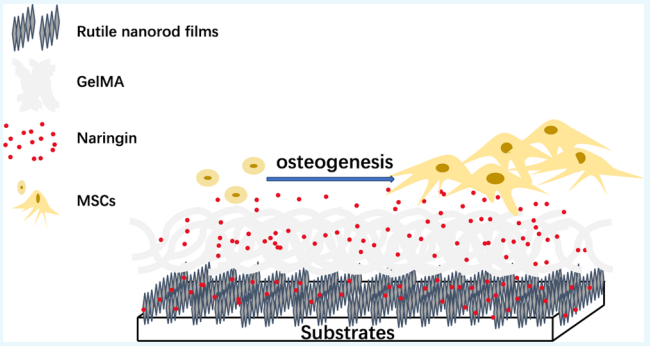

INTRODUCTION

Naringin, a Chinese traditional herb, is the main active component of *Rhizoma drynariae*. It has been demonstrated to be able to promote the adhesion, proliferation, and osteogenesis of cells.[1,2] The biological activities of naringin express a dose-dependent manner. For example, Liu et al. proved that naringin enhanced the proliferation and osteogenic differentiation of human amniotic fluid-derived stem cells in the range 1−100 μg/mL, while an inhibition effect occurred at 200 μg/mL.[3] Li et al. found that 10 μg/mL naringin showed the most remarkable effect on osteocalcin expression of rat bone marrow stromal cells.[4] Therefore, it is necessary to control the release of naringin to optimize its function.

Gelatin methacryloyl (GelMA) is one type of hydrogel biomaterials which attracts the attention to control the release of drug. Researchers have proved that GelMA could provide sustained and localized presentation of drug after a burst release.[5−7] Furthermore, GelMA has been demonstrated to regulate the fate of stem cells by mimicking the physiochemical properties of the extracellular matrix. Nichol et al. demonstrated that cells readily proliferated and elongated on the surface of GelMA hydrogel.[8] Fang et al. found that Bio-GelMA significantly enhanced proliferation and alkaline phosphatase (ALP) activity of encapsulated adipose-derived stem cells.[9] We, therefore, speculated that GelMA might be a suitable carrier to control the release of naringin and meanwhile promote the osteogenesis of stem cells. However, it remains to be discovered how to load naringin in GelMA and how to fix GelMA as a coating on the surface of biomaterials.

With the development of nanotechnologies, we have seen great progress in surface modification of implants during the past few years.[10] The TiO_2 film on the implant surface with good stability has attracted a lot of interest. TiO_2 nanorod films have been demonstrated to be osteo-conductivity.[11−13] Moreover, Ge et al. found that mesoporous bioactive glass incorporated with TiO_2 nanorod films could restrain the initial burst release of rhBMP-2 and improve rhBMP-2 function.[14] Thus, rutile nanorod films were selected here to fix GelMA.

In this study, naringin was loaded by two distinct manners in GelMA incorporated on TiO_2 nanorod coatings to realize controlled release. Also, a series of in vitro experiments were carried out to evaluate their activities for osteogenic differentiation of mesenchymal stem cells (MSCs).

Received: August 26, 2019
Accepted: October 30, 2019
Published: November 6, 2019

DOI: 10.1021/acsomega.9b02751
ACS Omega 2019, 4, 19350−19357

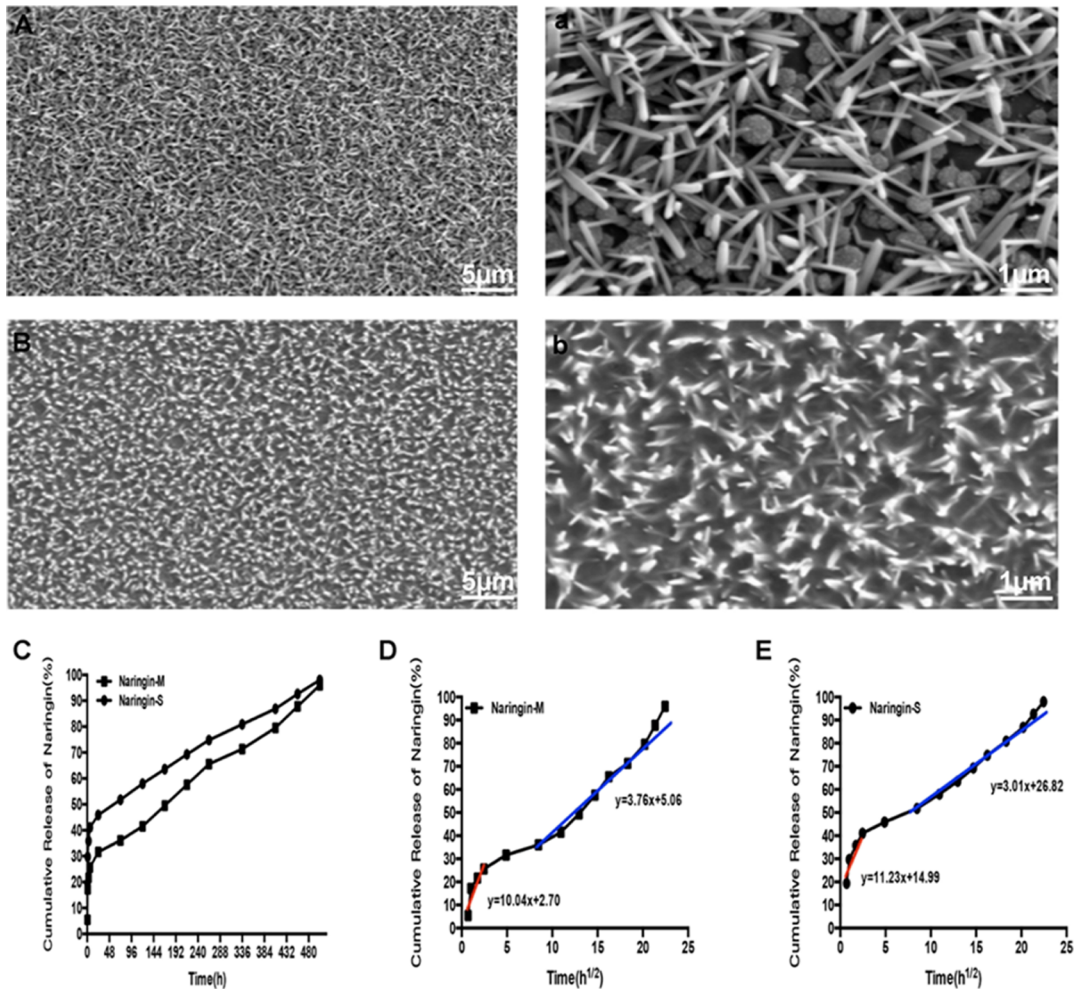

Figure 1. (A,a) SEM images of rutile nanorod films. (B,b) SEM images of GelMA-incorporated rutile nanorod films. (C) Release profile of naringin from naringin-M and naringin-S. (D,E) Corresponding linear fitting curves of release behaviors for naringin-M and naringin-S, respectively.

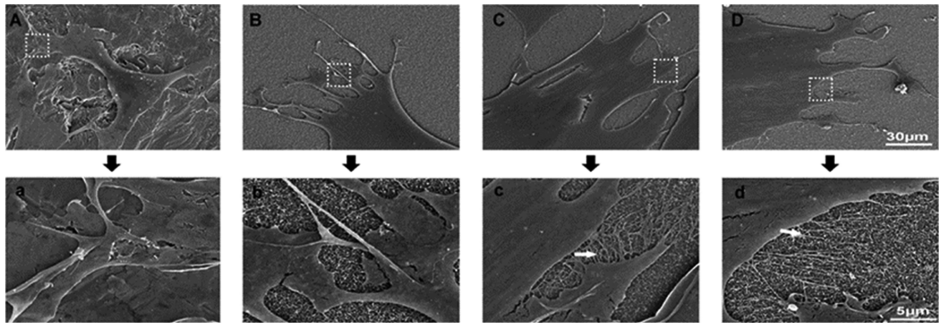

Figure 2. SEM images of MSC morphology on different substrates: (A) Ti, (B) GelMA, (C) naringin-M, and (D) naringin-S. (a−d) Enlarged images accordingly. Filopodia were indicated by the arrow.

RESULTS

The surface morphologies of TiO_2 nanorod coatings before and after GelMA incorporation were observed by scanning electron microscopy (SEM). As shown in Figure 1A, the dimension and height of nanorods were nearly 100 and 600 nm, respectively. These results were consistent with our previous work.[15] The distinct spacing between nanorods was further beneficial for the incorporation of GelMA (Figure 1B). As shown in Figure 1C, the release profile of naringin was sustained after an apparent burst release. We also analyzed the release kinetics (Figure 1D,E). During the first stage of burst release, the intercept represented the initial percentage of released naringin. The parameter was 2.70 for naringin-M and 14.99 for naringin-S, which suggested that more drug might be reserved in naringin-M. During the second stage of sustained release, the slope represented the rate of released behavior. The parameter was 3.76 for naringin-M and 3.01 for naringin-S, which revealed higher concentration of naringin released from naringin-M in unit time. According to the release kinetics, we inferred that these two typical coatings with distinct release kinetics of naringin could provide an ideal model to further explore their activities for osteogenic differentiation of MSCs.

DOI: 10.1021/acsomega.9b02751
ACS Omega 2019, 4, 19350−19357

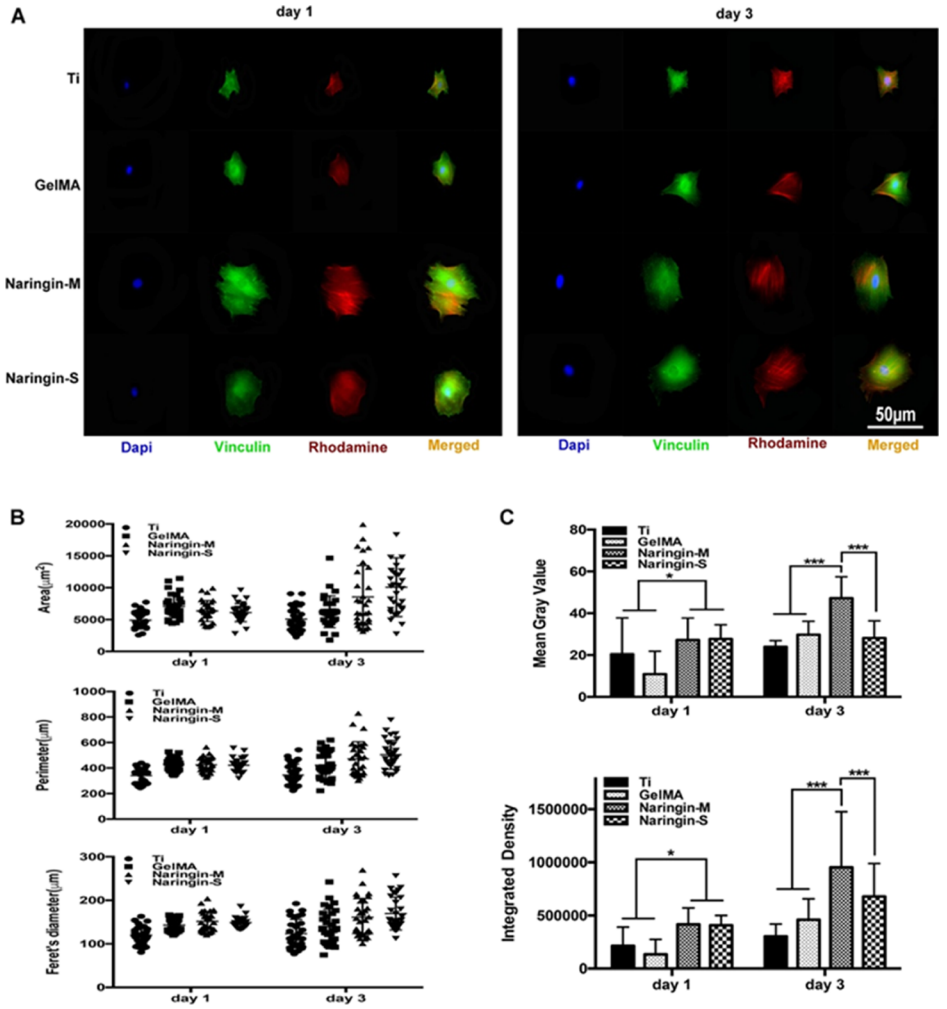

Figure 3. (A) Fluorescence images of typical cells on various substrates after 1 and 3 days of culture. The cells were stained for the focal adhesion protein vinculin (green), actin cytoskeleton (red), and cellular nuclei (blue). (B) Cytomorphometric evaluation of area, perimeter, and Feret's diameter. (C) Quantitative analysis of fluorescence intensity of focal adhesions (n = 30).

We first observed that the cellular morphology on various substrates. As shown in Figure 2, the morphology of MSCs cultured on naringin-M and naringin-S remarkably displayed more filopodia compared to that of the other two substrates. These results suggested that the coatings loaded with naringin promoted the spreading of MSCs.

Immunofluorescence was further employed to observe the adhesion behaviors of MSCs on various substrates. As shown in Figure 3A, the cellular area was larger on naringin-M and naringin-S compared to on that of cells on Ti and GelMA. Moreover, quantitative analysis also confirmed the obvious attachment and spreading of MSCs on the coatings loaded with naringin especially on day 3 (Figure 3B). It was worth to note that MSCs on naringin-M displayed more vinculin with higher fluorescence intensity than the others on day 3.

The cellular viability and proliferation were evaluated by using live/dead assay and CCK-8 assay. As shown in Figure 4A, the density of MSCs increased obviously on naringin-M and naringin-S. Especially the number of attached cells was significantly upregulated on naringin-M and naringin-S even after 5 days of culture. These results were further confirmed by the quantitative analysis of CCK-8 results (Figure 4B), which could be attributed to the bioactivity of naringin.

Assessment of osteogenesis genes was achieved by real-time polymerase chain reaction (PCR). The results are shown in Figure 5A. After 7 days of culture, all expressions of osteogenic-related genes were upregulated on naringin-M compared to the others. After 14 days of culture, there was no obvious difference between the coatings loaded with naringin, but expression of osteogenesis genes was notably upregulated when compared to Ti and GelMA. What is more, the larger area of ALP-positive with higher intensity displayed on naringin-M and naringin-S than on the two others after 7 days of culture as shown in Figure 5B. Moreover, the quantitative analysis revealed remarkably upregulated ALP activity on naringin-M (Figure 5C).

The ability of mineralization was evaluated by Alizarin Red Assay kit after long-term culture. The results are shown in Figure 6. The more obvious area of Alizarin-positive on naringin-M and naringin-S compared to on the two others. Furthermore, the quantitative analysis confirmed the significantly upregulated osteogenesis on naringin-M.

DISCUSSION

Recently, GelMA has been widely used to control the drug delivery. GelMA, acting as carriers, can interact with drug by physisorption and covalent linking. In general, drug delivery

DOI: 10.1021/acsomega.9b02751
ACS Omega 2019, 4, 19350−19357

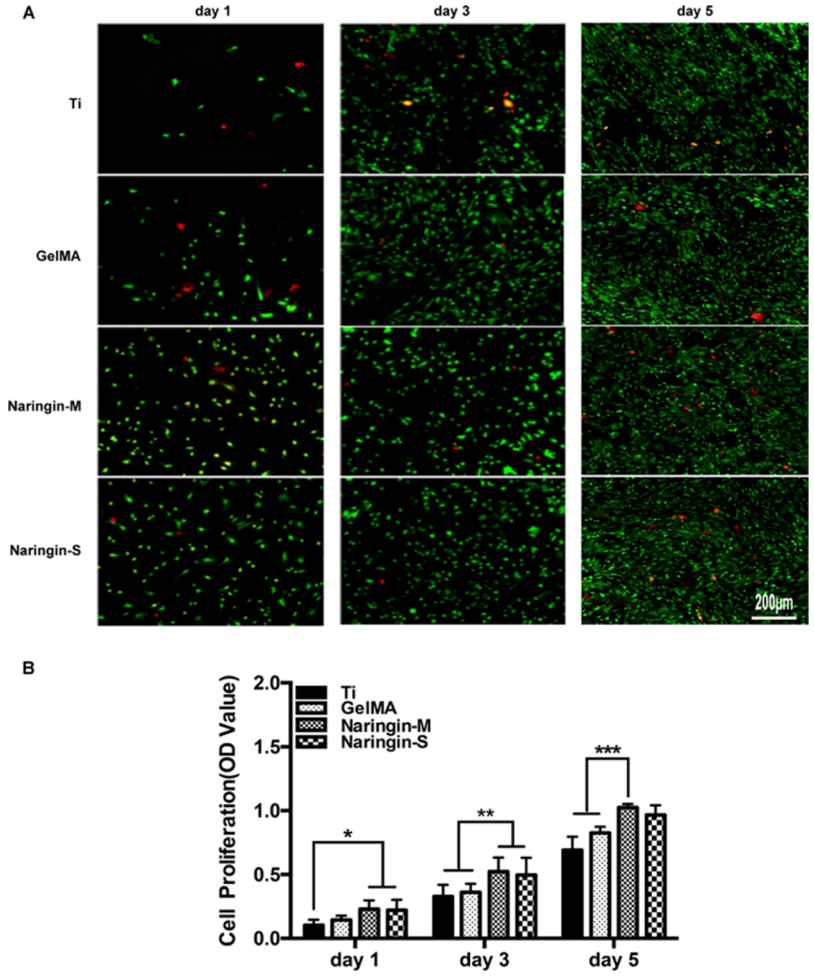

Figure 4. (A) Cell viability using staining-derived fluorescent images. The live cells were stained with calcein (green), and the dead cells were stained with ethidium (red). (B) CCK-8 assays.

from GelMA is mediated by diffusion and degradation.[16] At first, diffusion dominances the release profile because matrix degradation is slow.[17] Drug is immobilized by macro/nano-entrapment. Once GelMA is dissolved in the solvent, the diffusion of drug from the porous structure occurs. The molecular weight of drugs and the pore size of GelMA play important roles in the release process.[18−20] The degradation of GelMA can be divided into bulk and surface erosion.[16] Bulk erosion is homogenous when GelMA swelling is faster than the polymer disintegration. In contrast, surface erosion is heterogeneous when the polymer disintegration is predominant. A number of parameters are related in the process such as the chemical structure of GelMA, exposure time to UV light, the concentration of the GelMA hydrogel, and others.[21,22] In this work, we designed two coatings to achieve degradation-type release (naringin-M) and diffusion-type release (naringin-S). Naringin delivery was constant and sustained after a burst release from two coatings (Figure 1C). However, the release kinetics of two coating was different (Figure 1D,E). Because the molecular weight of naringin was low, the entrapped naringin could be released from the porous structure of GelMA easily. Therefore, the initial percentage of released naringin from naringin-S was higher than that of naringin-M.

Moreover, we demonstrated that the release of naringin was beneficial to the attachment (Figure 3), osteogenesis (Figure 5), and mineralization (Figure 6) of MSCs. Though the biological activities of naringin have been confirmed,[23−25] the mechanism of its osteo-conductivity is complicated and yet to be illuminated. Several studies manifested that extracellular regulated protein kinases (ERK) 1/2 were found to be activated by naringin, and osteogenic differentiation was repressed when the inhibitor of ERK 1/2 was used.[26,27] The activation of ERK 1/2 is downstream of the Ras family.[28] Lin et al. demonstrated that the Ras family was remarkably activated by naringin.[29] Furthermore, the ERK 1/2 pathway can regulate osteogenic differentiation through microRNA.[30] Meanwhile, GelMA hydrogels and collagen have also been demonstrated to regulate the osteogenic differentiation of MSCs via ERK signaling pathways.[31,32] In this study, the osteogenic differentiation potential of MSCs on naringin-M was more remarkable compared to that of naringin-S. For the naringin-S, the naringin was entrapped in the pore structure of GelMA and released quickly. When it comes to the naringin-M, the naringin not only physically absorbed on GelMA but also covalently bonded with GelMA during the curing process. Therefore, the detected concentration of naringin released from naringin-M was lower than that from naringin-S at the initial stage. Nonetheless, the synergistic release of naringin with degraded GelMA from naringin-M enhanced the osteogenic differentiation of MSCs more effectively. These results suggested that there might be a synergistic effect of naringin and GelMA to regulate the osteogenic differentiation

DOI: 10.1021/acsomega.9b02751
ACS Omega 2019, 4, 19350−19357

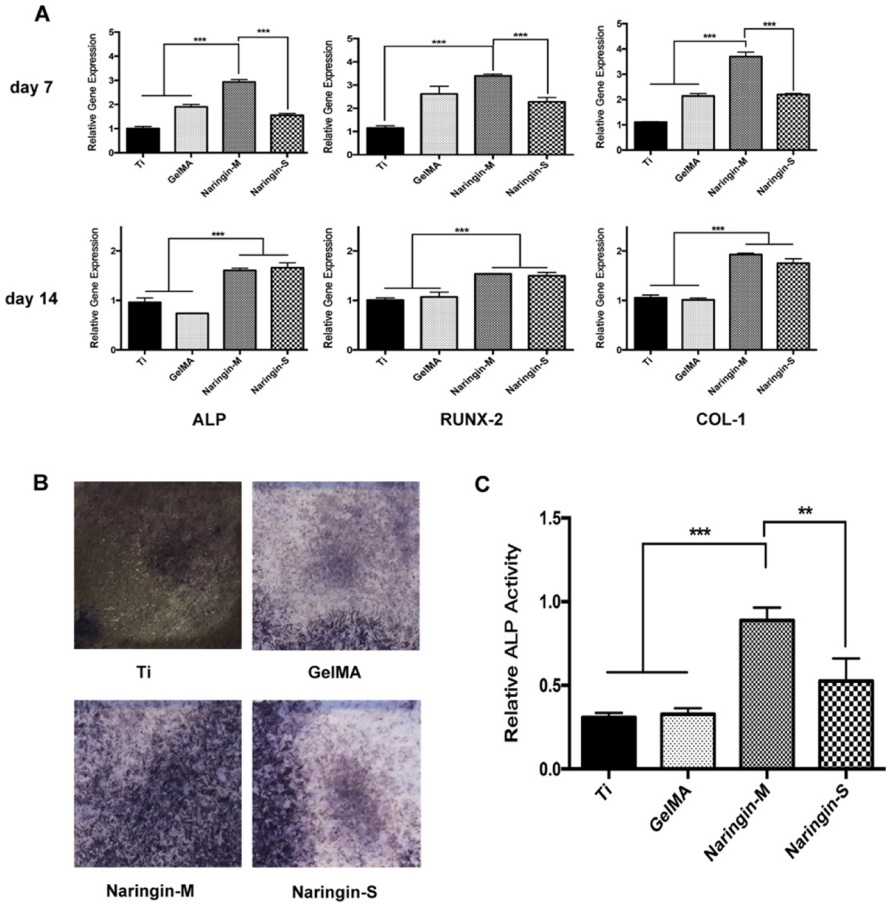

Figure 5. (A) Quantitative analysis of real-time PCR for relative expression of osteogenesis genes after 7 and 14 days of culture. (B) Images of ALP activity done by Alkaline Phosphatase Assay Kit after 7 days of culture. (C) Quantitative analysis of ALP activity.

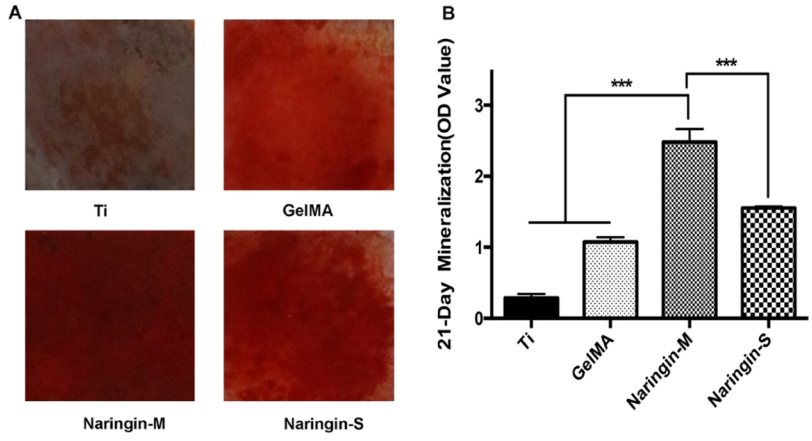

Figure 6. (A) Images of mineralization capacity achieved by Alizarin Red Assay Kit after 21 days of culture. (B) Corresponding quantitative analysis.

of MSCs because of the similar signaling pathway potentially involved, which needs further investigation.

CONCLUSIONS

In summary, we designed GelMA-incorporated rutile nanorod films loaded with naringin which enhanced osteogenesis of MSCs. The release behavior of naringin was shown to play a critical role in the fate of MSCs. Despite two distinct coatings could both control the release of naringin, the degradation-type release of naringin-M was demonstrated to enhance the osteogenic differentiation of MSCs more effectively. In all, our study may provide a potential strategy to achieve controlled release of naringin and stress osteogenic function of naringin.

EXPERIMENTAL SECTION

Preparation of the Four Typical Substrates. Four typical substrates were prepared as following: Ti, GelMA (the GelMA hydrogel incorporated rutile nanorod films), naringin-M (mixing naringin in the GelMA hydrogel), and naringin-S (soaking the obtained GelMA with the naringin solution).

DOI: 10.1021/acsomega.9b02751
ACS Omega 2019, 4, 19350−19357

Rutile nanorod films were prepared by two steps. First, quartz substrates (1 cm × 1 cm) were ultrasonically cleaned by acetone (Hushi), absolute ethanol (Hushi), and distilled water. Second, dissolved acetylacetone (62 μL; Aladdin), distilled water (36 μL), tetrabutyl titanate (680 μL; Aladdin), and polyvinylpyrrolidone (0.4 g; Ourchem) were diluted with ethanol into 10 mL. Then, 20 μL of the solution was spin-coated on the quartz substrate at the speed of 8000 rpm for 40 s. Finally, the substrates were calcinated at 700 °C for 1 h to get nanodot films. The nanorod films were further prepared by the following hydrothermal process. The hydrothermal solution was prepared by mixing the 49 mL HCl (Hushi) into 50 mL distilled water as well as the addition of 1020 μL tetrabutyl titanate. The reaction was carried out at 160 °C for 2.5 h. After the reaction, the substrates were calcinated at 700 °C for 1 h. The obtained nanorod films were then washed for three times using water and ethanol. The topography of substrates was observed by field-emission SEM (FE-SEM, Hitachi SU-70).

To prepare the GelMA coatings on the nanorod films (GelMA substrate), 50 μL of the GelMA hydrogel solution (5% GelMA hydrogel and 2.5 mg/mL type I collagen solution in the volume ratio of 10:1) was spin-coated on the rutile nanorod films at 8000 rpm for 40 s. The naringin-M substrate was prepared by mixing the naringin (Sigma) to the hydrogel solution to reach the final concentration of 1.4 g/L before spinning. Also, the naringin-S substrate was prepared by soaking the GelMA substrate in 1.4 g/L naringin solution.

Evaluation of the Release Behaviors. To study the release kinetics, naringin-M and naringin-S substrates were placed in a 24-multiwell plate each containing 500 μL phosphate buffer saline (PBS, Genom). At the corresponding point, the original PBS was collected for measurement by ultraviolet spectroscopy at 415 nm and another new 500 μL PBS was added to continue the release experiment. An empirical equation simplified from the Higuchi equation, $Q = kt^{1/2} + b$, was applied. Q represents the total released percentage after time t, k reveals the rate of release behavior, and b is the percentage of initial burst release.

Cell Culture and Seeding. MSCs were extracted from the bone marrow of the tibias and femur of Sprague-Dawley rats (Slaccas). MSCs were cultured in α-modified minimum essential medium (α-MEM; Genom) containing 10% fetal bovine serum (ScienCell) and 1% penicillin streptomycin (Genom) under a humidified atmosphere of 0.5% CO_2 at 37 °C. The P3−P5 of MSCs were digested with 0.25% trypsin (Genom) and seeded on the surface of four substrates with a density of 2×10^4 cells/well in a 24-multiwell plate each containing 500 μL of the cell suspension. The culture medium was renewed every other day.

Morphology of the Cells. The samples were fixed with 2.5% glutaraldehyde (Hushi) solution for 2 h at room temperature. Then, the samples were rinsed with PBS three times. After this, 1% osmic acid was used to fix the samples. The dehydration process was achieved by gradient ethanol of 50, 70, 80, 95, and 100%. The samples were dried and sprayed with gold. The morphology of cells was observed by field-emission SEM (Hitachi SU-70).

Immunostaining of the Cells. After 1 and 3 days of culture, the samples were fixed with 4% paraformaldehyde solution (Biosharp) for 20 min at room temperature. Then, the samples were rinsed with PBS three times. 1% Triton X-100 (Sigma) in PBS was supplemented to rupture cell membranes for 10 min at 4 °C and then washed with PBS. 2% bovine serum albumin (BSA, Biofrox) added with 2% FBS was used as the sealant at 4 °C for 1 h. Focal adhesions were stained with antivinculin monoclonal antibody (Sigma) in 2% BSA at 4 °C overnight. The samples were then rinsed with 0.05% Tween (Vetec) in PBS three times. The actin cytoskeleton was stained by rhodamine phalloidin. The cellular nuclei were stained using Dapi (Vector). Cells were visualized by confocal laser scanning microscopy (Nikon, Japan). The quantitative analysis was carried out using ImageJ software.

Cellular Viability. For live/dead staining of cells, substrates were first rinsed with PBS and then stained by calcein-AM and ethidium homodimer-1 for 30 min. Samples were observed by the inverted fluorescent microscope. For the CCK-8 assay, at the designed time points, 500 mL of the α-MEM medium and 50 mL of the CCK-8 (Dojindo) solution were added in each sample and incubated at 37 °C for 2 h. Finally, the absorbance was measured at 450 nm.

Gene Expression Analysis and ALP Activity. The cells seeded on four substrates were collected on day 7 and day 14. RNA was extracted by using TRIzol reagent (Invitrogen) and then was reversed into cDNA following DNAseI treatment. Real-time PCR was used to detect the indicated gene level of ALP, RUNX2, and COL-1. The primers were listed as following (Table 1).

Table 1. Primer Sequences for Real-Time PCR

gene	primer sequence (5′−3′)
ALP	F: CGTCTCCATGGTGGATTATGCT, R: CCCAGGCACAGTGGTCAAG
RUNX-2	F: GCTTCTCCAACCCACGAATG, R: GAACTGATAGGACGCTGACGA
COL-1	F: TCCTGCCGATGTCGCTATC, R: CAAGTTCCGGTGTGACTCGTG
GAPDH	F: GGCACAGTCAAGGCTGAGAATG, R: ATGGTGGTGAAGACGCCAGTA

For the ALP activity, by the end of day 7, ALP Assay Kit (Beyotime) was used to evaluate the ALP activity according to the manufacturer protocol. Also, the resulting optical density values were detected at 405 nm.

Evaluation of Mineralization. After 21 days of culture, the samples were fixed using 70% ethanol for 1 h at room temperature and incubated with 1% Alizarin Red S (Sigma) for 20 min. The calcium nodule was observed by camera. After this, the samples were incubated in PBS for 15 min and then in 10% cetylpyridinium chloride (Aladdin) for 15 min. The quantitative analysis was achieved by measuring the absorbance at 560 nm.

Statistical Analysis. The data were expressed as the mean ± standard error of the mean. Statistical significance test was determined using ANOVA followed by Student's t-test. $^*P < 0.5$, $^{**}P < 0.01$, and $^{***}P < 0.001$ were considered to be statistically different.

AUTHOR INFORMATION

Corresponding Authors

*E-mail: whmwhm@zju.edu.cn (H.W.).
*E-mail: yumengfei@zju.edu.cn (M.Y.).
*E-mail: lingqingdong@zju.edu.cn (L.D.).

ORCID

Kui Cheng: 0000-0003-4828-6450

DOI: 10.1021/acsomega.9b02751
ACS Omega 2019, 4, 19350−19357

Wenjian Weng: 0000-0002-9373-7284
Mengfei Yu: 0000-0002-7700-4697
Lingqing Dong: 0000-0002-2203-3212

Author Contributions

M.Y. and L.D. conceived and designed the experiments. Y.S. and D.Y. carried out the experiments. Y.S., D.Y., Y.L., B.Y., J.L., K.C., W.W., H.W., M.Y., and L.D. analyzed the data. Y.S. and L.D. wrote the manuscript. All the authors commented on the manuscript.

Notes

The authors declare no competing financial interest.

■ ACKNOWLEDGMENTS

This work was financially supported by the National Natural Science Foundation of China (81600838, 81873720, 81670972, 51772273), Key Research and Development Program of Zhejiang, China (2017C01054, 2018C03062), the 111-Project under grant no. B16042, the Medical Technology and Education of Zhejiang Province of China (2016KYB178, 2018KY501), the Zhejiang Provincial Natural Science Foundation (LY15E020004), the Zhejiang Provincial Chinese Medical Science Research Foundation (2016ZB077), the National Key Research and Development Program of China (2016YFC0902702), and the Hangzhou Science and Technology Development Plan (20171226Y50).

■ REFERENCES

(1) Yin, L.; Cheng, W.; Qin, Z.; Yu, H.; Yu, Z.; Zhong, M.; Sun, K.; Zhang, W. Effects of Naringin on Proliferation and Osteogenic Differentiation of Human Periodontal Ligament Stem Cells In Vitro and In Vivo. *Stem Cells Int.* **2015**, *2015*, 1.

(2) Wong, K.-C.; Pang, W.-Y.; Wang, X.-L.; Mok, S.-K.; Lai, W.-P.; Chow, H.-K.; Leung, P.-C.; Yao, X.-S.; Wong, M.-S. Drynaria fortunei-derived total flavonoid fraction and isolated compounds exert oestrogen-like protective effects in bone. *Br. J. Nutr.* **2013**, *110*, 475−485.

(3) Liu, M.; Li, Y.; Yang, S.-T. Effects of naringin on the proliferation and osteogenic differentiation of human amniotic fluid-derived stem cells. *J. Tissue Eng. Regener. Med.* **2017**, *11*, 276−284.

(4) Xu, Z.; Li, N. Naringin promotes osteoblast differentiation and effectively reverses ovariectomy-induced osteoporosis. *J. Orthop. Sci.* **2013**, *18*, 478−485.

(5) Sun, X.; Zhao, X.; Zhao, L.; Li, Q.; D'Ortenzio, M.; Nguyen, B.; Xu, X.; Wen, Y. Development of a hybrid gelatin hydrogel platform for tissue engineering and protein delivery applications. *J. Mater. Chem. B* **2015**, *3*, 6368−6376.

(6) Samorezov, J. E.; Headley, E. B.; Everett, C. R.; Alsberg, E. Sustained presentation of BMP-2 enhances osteogenic differentiation of human adipose-derived stem cells in gelatin hydrogels. *J. Biomed. Mater. Res., Part A* **2016**, *104*, 1387−1397.

(7) Li, Y.; Yan, D.; Fu, F.; Liu, Y.; Zhang, B.; Wang, J.; Shang, L.; Gu, Z.; Zhao, Y. Composite core-shell microparticles from microfluidics for synergistic drug delivery. *Sci. China Mater.* **2017**, *60*, 543−553.

(8) Nichol, J. W.; Koshy, S. T.; Bae, H.; Hwang, C. M.; Yamanlar, S.; Khademhosseini, A. Cell-laden microengineered gelatin methacrylate hydrogels. *Biomaterials* **2010**, *31*, 5536−5544.

(9) Fang, X.; Xie, J.; Zhong, L.; Li, J.; Rong, D.; Li, X.; Ouyang, J. Biomimetic gelatin methacrylamide hydrogel scaffolds for bone tissue engineering. *J. Mater. Chem. B* **2016**, *4*, 1070−1080.

(10) Bauer, S.; Schmuki, P.; von der Mark, K.; Park, J. Engineering biocompatible implant surfaces. *Prog. Mater. Sci.* **2013**, *58*, 261−326.

(11) Yu, M.-L.; Yu, M.-F.; Zhu, L.-Q.; Wang, T.-T.; Zhou, Y.; Wang, H.-M. The Effects of TiO2Nanodot Films with RGD Immobilization on Light-Induced Cell Sheet Technology. *BioMed Res. Int.* **2015**, *2015*, 1.

(12) Qiu, J.; Li, J.; Wang, S.; Ma, B.; Zhang, S.; Guo, W.; Zhang, X.; Tang, W.; Sang, Y.; Liu, H. TiO2 Nanorod Array Constructed Nanotopography for Regulation of Mesenchymal Stem Cells Fate and the Realization of Location-Committed Stem Cell Differentiation. *Small* **2016**, *12*, 1770−1778.

(13) Li, Z.; Qiu, J.; Du, L. Q.; Jia, L.; Liu, H.; Ge, S. TiO_2 nanorod arrays modified Ti substrates promote the adhesion, proliferation and osteogenic differentiation of human periodontal ligament stem cells. *Mater. Sci. Eng., C* **2017**, *76*, 684−691.

(14) Ge, F.; Yu, M.; Yu, C.; Lin, J.; Weng, W.; Cheng, K.; Wang, H. Improved rhBMP-2 function on MBG incorporated TiO_2 nanorod films. *Colloids Surf., B* **2017**, *150*, 153−158.

(15) Cheng, K.; Yu, M.; Liu, Y.; Ge, F.; Lin, J.; Weng, W.; Wang, H. Influence of integration of TiO2 nanorods into its nanodot films on pre-osteoblast cell responses. *Colloids Surf., B* **2015**, *126*, 387−393.

(16) van Tienderen, G. S.; Berthel, M.; Yue, Z.; Cook, M.; Liu, X.; Beirne, S.; Wallace, G. G. Advanced fabrication approaches to controlled delivery systems for epilepsy treatment. *Expert Opin. Drug Delivery* **2018**, *15*, 915−925.

(17) Tarafder, S.; Bose, S. Polycaprolactone-coated 3D printed tricalcium phosphate scaffolds for bone tissue engineering: in vitro alendronate release behavior and local delivery effect on in vivo osteogenesis. *ACS Appl. Mater. Interfaces* **2014**, *6*, 9955−9965.

(18) Lai, T. C.; Yu, J.; Tsai, W. B. Gelatin methacrylate/carboxybetaine methacrylate hydrogels with tunable crosslinking for controlled drug release. *J. Mater. Chem. B* **2016**, *4*, 2304−2313.

(19) Celikkin, N.; Mastrogiacomo, S.; Jaroszewicz, J.; Walboomers, X. F.; Swieszkowski, W. Gelatin methacrylate scaffold for bone tissue engineering: The influence of polymer concentration. *J. Biomed. Mater. Res., Part A* **2018**, *106*, 201−209.

(20) Wu, W.; Dai, Y.; Liu, H.; Cheng, R.; Ni, Q.; Ye, T.; Cui, W. Local release of gemcitabine via in situ UV-crosslinked lipid-strengthened hydrogel for inhibiting osteosarcoma. *Drug Delivery* **2018**, *25*, 1642−1651.

(21) Serafim, A.; Tucureanu, C.; Petre, D.-G.; Dragusin, D.-M.; Salageanu, A.; Van Vlierberghe, S.; Dubruel, P.; Stancu, I.-C. One-pot synthesis of superabsorbent hybrid hydrogels based on methacrylamide gelatin and polyacrylamide. Effortless control of hydrogel properties through composition design. *New J. Chem.* **2014**, *38*, 3112−3126.

(22) Luo, Z.; Sun, W.; Fang, J.; Lee, K.; Li, S.; Gu, Z.; Dokmeci, M. R.; Khademhosseini, A. Biodegradable Gelatin Methacryloyl Microneedles for Transdermal Drug Delivery. *Adv. Healthc. Mater.* **2019**, *8*, 1801054.

(23) Li, L.; Zeng, Z.; Cai, G. Comparison of neoeriocitrin and naringin on proliferation and osteogenic differentiation in MC3T3-E1. *Phytomedicine* **2011**, *18*, 985−989.

(24) Yang, S.-Y.; Li, N.; Xu, Z.; Wooley, P. H.; Zhang, J. Therapeutic potentials of naringin on polymethylmethacrylate induced osteoclastogenesis and osteolysis, in vitro and in vivo assessments. *Drug Des., Dev. Ther.* **2014**, *8*, 1−11.

(25) Li, C. H.; Wang, J. W.; Ho, M. H.; Shih, J. L.; Hsiao, S. W.; Thien, D. V. H. Immobilization of naringin onto chitosan substrates by using ozone activation. *Colloids Surf., B* **2014**, *115*, 1−7.

(26) Wang, H.; Li, C.; Li, J.; Zhu, Y.; Jia, Y.; Zhang, Y.; Zhang, X.; Li, W.; Cui, L.; Li, W.; Liu, Y. Naringin enhances osteogenic differentiation through the activation of ERK signaling in human bone marrow mesenchymal stem cells. *Iran. J. Basic Med. Sci.* **2017**, *20*, 408−414.

(27) Wei, K.; Xie, Y.; Chen, T.; Fu, B.; Cui, S.; Wang, Y.; Cai, G.; Chen, X. ERK1/2 signaling mediated naringin-induced osteogenic differentiation of immortalized human periodontal ligament stem cells. *Biochem. Biophys. Res. Commun.* **2017**, *489*, 319−325.

(28) Kim, D.-I.; Lee, S.-J.; Lee, S.-B.; Park, K.; Kim, W.-J.; Moon, S.-K. Requirement for Ras/Raf/ERK pathway in naringin-induced G1-cell-cycle arrest via p21WAF1 expression. *Carcinogenesis* **2008**, *29*, 1701−1709.

DOI: 10.1021/acsomega.9b02751
ACS Omega 2019, 4, 19350−19357

(29) Lin, F.; Zhu, Y.; Hu, G. Naringin promotes cellular chemokine synthesis and potentiates mesenchymal stromal cell migration via the Ras signaling pathway. *Exp. Ther. Med.* **2018**, *16*, 3504−3510.
(30) Hu, N.; Feng, C.; Jiang, Y.; Miao, Q.; Liu, H. Regulative Effect of Mir-205 on Osteogenic Differentiation of Bone Mesenchymal Stem Cells (BMSCs): Possible Role of SATB2/Runx2 and ERK/MAPK Pathway. *Int. J. Mol. Sci.* **2015**, *16*, 10491−10506.
(31) Yue, K.; Trujillo-de Santiago, G.; Alvarez, M. M.; Tamayol, A.; Annabi, N.; Khademhosseini, A. Synthesis, properties, and biomedical applications of gelatin methacryloyl (GelMA) hydrogels. *Biomaterials* **2015**, *73*, 254−271.
(32) Salasznyk, R. M.; Klees, R. F.; Hughlock, M. K.; Plopper, G. E. ERK Signaling Pathways Regulate the Osteogenic Differentiation of Human Mesenchymal Stem Cells on Collagen I and Vitronectin. *Cell Commun. Adhes.* **2004**, *11*, 137−153.

DOI: 10.1021/acsomega.9b02751
ACS Omega 2019, 4, 19350−19357